Published in final edited form as:
Neuroimage. 2008 February 1; 39(3): 1129–1141. doi:10.1016/j.neuroimage.2007.09.042.

A Method for Multi-group Inter-Participant Correlation: Abnormal Synchrony in Patients with Schizophrenia during Auditory Target Detection

D. Kim[1], **G. D. Pearlson**[3,4], **K. A. Kiehl**[1], **E. Bedrick**[5], **O. Demirci**[1], and **V. D. Calhoun**[1,2,3]

[1]The MIND Institute, Albuquerque, NM 87131

[2]Department of Electrical and Computer Engineering, University of New Mexico, Albuquerque, NM 87131

[3]Dept. of Psychiatry, Yale University, New Haven, CT 06520

[4]Olin Neuropsychiatry Research Center, Hartford, CT 06106

[5]Department of Mathematics and Statistics, University of New Mexico, Albuquerque, NM 87131

Abstract

The general linear model (GLM) approach is the most commonly used method in functional magnetic resonance imaging analysis to predict a particular response. Recently, a novel method of analysis, referred to as inter-participant correlation (IPC), was developed that attempts to determine the level of BOLD (Blood Oxygen Level Dependent) synchrony among subjects. The IPC approach enables detection of changes in inter-participant BOLD synchrony in a manner that does not rely on an explicit model of the hemodynamic activity. In this paper, we extend IPC to the case of two groups and derive an approach for thresholding the resulting maps. We demonstrate our approach by comparing 35 patients with paranoid schizophrenia (DSM-IV subtype 295.30) to 35 healthy matched controls during an auditory target detection paradigm. Results showed significantly lower inter-participant BOLD synchrony in patients versus healthy controls in areas including bilateral temporal lobes, medial frontal gyrus, anterior cingulate cortex, dorsolateral prefrontal cortex, thalamus, insula, and cerebellum. The IPC approach is straightforward to use and provides a useful complement to traditional GLM techniques. This approach may also be sensitive to underlying, but unpredictable, changes in inter-participant BOLD synchrony between patients and controls.

Keywords

schizophrenia; paranoid; neural synchrony; fMRI; functional; brain; correlation; model; hemodynamic; GLM

Correspondence: Vince Calhoun, The MIND Institute, 1101 Yale Boulevard NE, Albuquerque, NM 87131, PH: 860-545-7768, E-mail: vcalhoun@unm.edu, Dae Il Kim, The MIND Institute, 1101 Yale Boulevard NE, Albuquerque, NM 87131, PH: 646-675-9193, E-mail: dkim@themindinstitute.org.

INTRODUCTION

The most commonly used technique in functional magnetic resonance imaging (fMRI) analysis is based on the general linear model (GLM) (Friston, et al. 1995a; Friston, et al. 1995c) and involves fitting the acquired fMRI data to a canonical hemodynamic response function (Friston, et al. 1995b; Rajapakse, et al. 1998). The GLM is an excellent tool when searching for a task-related response, but is limited by the fact that it only accounts for canonical hemodynamic activity. Recently, a novel approach to fMRI analysis, referred to as inter-participant correlation (IPC), was introduced that attempts to quantify the level of correlation of fMRI BOLD activity within a group of participants (Hejnar, et al. 2006). By not making a specific assumption about the shape of the hemodynamic response, the IPC approach has proven capable of revealing regions synchronized across individuals, and thus finding activations that do not necessarily track smoothly with a given task. More specifically, it attempts to determine this correlation at the voxel level between two participants for every voxel in the brain. A correlation map is then generated that depicts areas of high BOLD correlation between two participants and repeated for all possible pairwise comparisons within a group. The statistical average of these comparisons then provide a picture of which regions in the brain are synchronized for a particular group of participants.

The previous study that developed the IPC algorithm analyzed a single group of healthy controls. Here we develop the IPC method to allow for group comparisons and to make additional changes that would more effectively account for the variances between them. Two modifications were made to the original IPC algorithm. The first modification was to utilize the fundamental theories of U-statistics to create valid statistical thresholds for the within-group and between-group comparisons. The motivation for this modification was due to the fact that the previous algorithm divided its averaged correlation maps by its standard deviation and was thresholded at an arbitrary z-value. To remedy this, we took into account the dependence that would exist between individual correlation images as a result of performing an exhaustive correlation analysis between participants within a group. Our solution involved the use of U-statistics (Randles and Wolfe, 1979), a statistical method used in nonparametric statistics that accounted for the dependence between participants and provided us with true t-values that can be further thresholded using a false discovery rate correction (Genovese, et al. 2002). The second modification was made to account for the variances that might exist between sessions by using an ordinary GLM regression model to regress one participant's session with another. The original IPC algorithm concatenated the sessions for a single participant as a single session and then performed its correlation afterwards. The GLM regression model allows us to treat each session individually, thus the first session for each participant would be correlated with the first session of the other participant.

After the IPC results were generated, a clustering analysis was performed at the group-level to conglomerate regions that activate in a similar manner. This was performed to account for the possibility that neighboring voxels might have very different timecourses from one another since the IPC does not test for inter-voxel synchrony. The clustering approach allows us to see which regions of the brain are closely linked to one another and a maximum efficiency algorithm was developed to determine the best number of clusters to use for this part of the analysis.

In order to test the between-group comparisons approach with the IPC method, we chose to compare a group of patients with schizophrenia (n=35) with a matched group of healthy controls (n=35). Participants performed an auditory target detection or 'oddball' task. This task was chosen because this paradigm elicits a robust fMRI response that reliably distinguishes patients with schizophrenia from controls (Calhoun, et al. 2006; Kiehl and Liddle 2001; Kiehl, et al. 2005a; Laurens, et al. 2005; Ngan, et al. 2003). The auditory oddball paradigm is a task

where a participant hears a combination of three distinct classes of stimuli, defined as standard (80% probability), novel (10% probability), and target (10% probability) tones. The participant is instructed to press a button during the experiment whenever they hear a target tone and to ignore everything else. Previous work utilizing this paradigm with fMRI have found attenuated activity in schizophrenia within frontal, temporal, parietal, and subcortical sites during the detection process of this specific target auditory tone (Kiehl, et al. 2005b).

Our specific hypothesis was that deficits in schizophrenia that are related to abnormalities within the delicate interplay of multiple brain regions could manifest as a lack of coherence between participants¨ This is consistent with the hypothesis that patients with schizophrenia are characterized by abnormal interconnections between various brain regions (Breakspear, et al. 2003; Friston 1998; Job, et al. 2002; Kubicki, et al. 2007). Calhoun et al. (2003) used independent component analysis to show that patients with schizophrenia were characterized by aberrant patterns of connectivity in bilateral temporal lobes during performance of the auditory oddball task. We hypothesized that healthy controls would show a much stronger correlation in BOLD activity versus patients with schizophrenia in the superior temporal gyrus and in areas associated with target detection such as the anterior cingulate, dorsolateral prefrontal cortex and subcortical systems such as the thalamus and cerebellum. (Calhoun, et al. 2004; Kiehl, et al. 2005a; Lawrie, et al. 2002; Stevens, et al. 2005).

METHODS

Participants

Thirty-five outpatients with schizophrenia (30 males) and thirty-five matched healthy controls (30 males) provided written informed consent and volunteered for the study. Healthy controls were free from any Axis I disorder, as assessed with the SCID (Structured Clinical Interview for DSM-IV-TR) screening device. Patients met criteria for paranoid schizophrenia (sub-type 295.30) in the DSM-IV based on a structured clinical interview and review of the case file (First et al., 1995). All participants were right handed and there were no significant group differences in age (patients, 38 ± 11 years, range 18–59 years; controls, 37 ± 12 years, range 18–55 years). IQ (Intelligence Quotient) assessments were determined from NART (National Adult Reading Test) scores where healthy controls were higher than patients (patients n=26, 35 ± 15 points; controls n=17, 22 ± 7 points; $t(41)=3.1323$, $p < .0032$). To determine the presence/absence of psychotic symptoms, the mean PANSS (Positive and Negative Syndrome Scale) for patients were determined (n=28, 66 ± 19.6). Medication information was available for 24 patients, where 13 patients were on atypical antipsychotic medications, 4 were on typical antipsychotic medications, 2 were on both atypical and typical medications, and three were on no medications at all. Four participants from the patient group were omitted from analysis, as they demonstrated extremely poor performance on the auditory oddball task (more than ten total incorrect responses in either targets or novels for both sessions). Two additional participants were omitted for excessive head motion (greater than one and a half voxel-length (6mm) in translation or rotation). All participants had normal hearing (assessed by self-report) and were able to carry out both tasks successfully during practice, and during the scanning session.

Tasks: Auditory Oddball

The auditory oddball task used in this study was identical to that used in the original inter-participant correlation study (Hejnar, et al. 2006). Two runs of auditory stimuli were presented to each participant by a computer stimulus presentation system (VAPP: http://nilab.psychiatry.ubc.ca/vapp/) via insert earphones embedded within 30 dB sound attenuating MR compatible headphones. The standard stimulus was a 500 Hz tone, the target stimulus was a 1000 Hz tone, and the novel stimuli consisted of non-repeating random digital

noises (e.g., tone sweeps, whistles). The target and novel stimuli each occurred with a probability of 10%; the non-target stimuli occurred with a probability of 80%. The stimulus duration was 200 ms with a random 1000, 1500, or 2000 ms inter-stimulus interval. All stimuli were presented at approximately 80 decibels and all participants reported that they could hear the stimuli and discriminate them from the background scanner noise. The headphones were designed to work together with the head restraint system in order to minimize head movement.

An MRI compatible fiber-optic response device (Lightwave Medical, Vancouver, B.C.) was used to acquire behavioral responses. Prior to entry into the scanning room, each participant performed a practice block of 10 trials to ensure understanding of the instructions. The participants were instructed to respond as quickly and accurately as possible with their right index finger every time they heard the target stimulus and not to respond to the non-target stimuli nor the novel stimuli.

Imaging Parameters

Imaging was implemented on a 3T Siemens Allegra MR system. Conventional spin-echo T_1 weighted sagittal localizers were acquired to view the positioning of the participant's head in the scanner and to graphically prescribe the functional image volumes. Functional image volumes were collected with a gradient-echo sequence (TR=1500 ms, TE=27 ms, FA=60°, FOV= 22 × 22 cm, 64 × 64 matrix, 4 kHz bandwidth, 3.44 by 3.44 mm in plane resolution, 4 mm slice thickness, 1 mm gap, 29 slices acquired axially) effectively covering the entire brain (145 mm) in an ascending manner. There were two runs of 255 time points each, prefaced by a 9 second rest block allowing T_1 effects to stabilize.

Data Analysis: Pre-processing

Data was preprocessed using the software package SPM2 (http://www.fil.ion.ucl.ac.uk/spm/). Images were realigned using INRIalign – a motion correction algorithm unbiased by local signal changes (Freire and Mangin 2001; Freire *et al*., 2002). Data was spatially normalized (Ashburner and Friston 1999) into the standard Montreal Neurological Institute space and spatially smoothed with a 10×10×10 mm^3 full width at half-maximum Gaussian kernel. The data (originally collected at 3.44×3.44×5 mm^3) was slightly sub-sampled to 3 mm^3, resulting in 53×63×46 voxels and a fifth-order infinite impulse response Butterworth low-pass filter of . 25 Hz was applied to remove high-frequency noise.

Inter-Participant Correlation

The algorithm used to analyze the data was based on the inter-participant correlation algorithm originally developed by (Hejnar, et al. 2006), but with two major modifications that will be discussed later in this section. The original algorithm calculated an inter-participant Pearson correlation for each voxel between all pairwise combinations of participants over their respective time-courses. For example, a voxel from subject #1 would be correlated with the same voxel from subject #2, but not with any other voxels. Every voxel in the brain is correlated this way, which generates a single correlation map for those two subjects. The total number of pair-wise correlation maps can be determined by the formula: $(n^2-n)/2$ where n is equal to the number of subjects. Thus, within a group of thirty-five subjects, there would be a total of 595 unique pair-wise correlation maps. These maps were then averaged together to create a total of thirty-five correlation maps, one for each particular subject. For statistical display purposes, the averaged maps were then divided by their standard deviation and an empirical threshold of z = 3 was used to find significant areas of correlation for each individual subject¨ However, the correlation maps were not divided by their standard deviation or thresholded for the second-level analysis. A sample correlation map for one healthy control is shown to exhibit the individual subject results obtained from the IPC algorithm (Figure 1).

The first modification was made to the original algorithm by using a multiple regression model to account for variances between runs. In the original approach, the sessions for each subject's dataset were concatenated and were analyzed as a single vector (e.g. $\mathbf{y} = \beta\mathbf{x}+\mathbf{e}$ where $\mathbf{x} = [\mathbf{x}_{run1}\ \mathbf{x}_{run2}]$ and $\mathbf{y} = [\mathbf{y}_{run1}\ \mathbf{y}_{run2}]$ contain de-trended data for one voxel for participants **x** and **y**; the square root of the multiple correlation coefficient, *R* is then computed for each pair of participants). The current approach creates a general linear model to regress both sessions of one subject's data onto another subject's data (allowing for variation between runs) as:

$$\begin{bmatrix} y_{run1} \\ y_{run2} \end{bmatrix} = \begin{bmatrix} \beta_1 \\ \beta_2 \end{bmatrix} \begin{bmatrix} x_{run1} & 0 \\ 0 & x_{run2} \end{bmatrix} + \begin{bmatrix} e_{run1} \\ e_{run2} \end{bmatrix},$$

where again, for this regression equation, the square root of the multiple correlation coefficient is computed for each pair of participants and used as our measure of correlation. If, for a given voxel, the pairwise correlation for participant *i* and *j* is $R_{i,j}$, we compute the within-subject average for subject *j* as $\overline{R}_j = \frac{\sum_i R_{i,j}}{(n-1)}$. The second modification, described in the next paragraph, involves extending the IPC approach to allow for group comparisons.

Second-Level Analysis (U-Statistics)

The average of all pairwise correlation maps for a given group (595 in total) was analyzed using a statistical model that accounts for dependencies that might exist between the participants' correlation maps. A specialized statistical approach was needed because, for example, a standard t-test on the average pairwise correlation will inevitably produce p-values that are too small if the dependence between two pairwise correlations that have one participant in common is ignored. The theory of U-statistics (Randles and Wolfe, 1979), which play an important role in the field of non-parametric statistics, provides an exact expression for the variance of the average pair-wise correlation and its large sample distribution. This approach allowed us to produce valid standard errors for one-sample and two-sample t-tests. The t-statistics could then be converted to p-values and false discovery rate (FDR) methods can be applied to account for multiple comparisons (Genovese, et al. 2002).

In the within-group analysis, let $\bar{r}$ be the sample average pair-wise correlation across all pairs of subjects (in this case 595 correlations). Then $\bar{r}$ is an unbiased estimate of ρ, the average of the pairwise correlations in the target population. Further, $\bar{r}$ is a U-statistic with a second order kernel so the Central Limit Theorem for U-statistics implies that the distribution of $\bar{r}$ is approximately normal for large values of *n*, the number of subjects. This limit theorem applied in conjunction with Slutsky's theorem implies that when *n* is large:

$$\frac{\bar{r}-\rho}{SE(\bar{r})} \dot{\sim} N(0,1)$$

where

$$SE(\bar{r}) = \sqrt{\frac{4(n-2)\widehat{\zeta_1}+2\widehat{\zeta_2}}{n(n-1)}}$$

is the estimated standard error of $\bar{r}$. Here, $\hat{\zeta}_2$ is the sample variance of all pair-wise correlations and $\hat{\zeta}_1$ is computed by subtracting r^{-2} from the average of all products of two pairwise correlations that have one participant in common.

The within-group analysis described above can also be applied to a between-group analysis since the samples are assumed to be selected independently and thus:

$$\frac{(\bar{r}_T - \bar{r}_C) - (\rho_T - \rho_C}{SE(\bar{r}_T - \bar{r}_C)} \sim N(0, 1)$$

where

$$SE^2(\bar{r}_T - \bar{r}_C) = SE^2(\bar{r}_T) + SE^2(\bar{r}_C).$$

The subscripts *T* and *C* are used to distinguish summaries that are computed separately from the treatment and control groups.

Finally, a contiguity filter was used in the final image to remove voxel clusters that were smaller than five voxels in terms of volume to filter out insignificant correlations and for display purposes.

Clustering

Finally, voxels with high correlations may have very different time-courses (since the only requirement for a high correlation is that the time-courses are similar for all participants). The template mask that was to be used for the clustering was generated from the two-sample group comparison IPC results. This mask was then used to select voxels from all the preprocessed fMRI datasets for our study and analyzed using the Calinski and Harabasz (CH) stopping rule (Harabasz 1974) to determine the optimal number of clusters or groupings that can be found.

To determine the optimal number of clusters, the distance between every two nodes (voxels) is calculated where the nodes were represented using the subjects and their activation time progress for the voxels. We then built the minimal spanning tree by a greedy algorithm. Then the CH measure is calculated as a ratio between the cluster sum of squares and the within-cluster sum of squares to obtain a range of numbers for cluster selection. The optimum number of clusters, which turned out to be 5, was finally determined as the number where we had no further increase in the CH measure.

In order to examine these time-courses, a k-means clustering algorithm was used on the auditory oddball task correlation data (Duda 2001). The algorithm was configured to find five clusters within the same template mask that was utilized for the Calinski and Harabasz analysis and then overlaid on an anatomical map for display purposes.

Event related averages were also calculated for targets, novels, and standards within each cluster for patients and healthy controls. Data from nine timepoints after the onset of each stimulus were taken from the k-means clustering results and averaged together for each cluster to determine their event related averages. These were then plotted for each cluster within a single plot to represent the overall effect of the hemodynamic response during target responses.

RESULTS

Behavioral Data

There were no significant differences between patients and healthy controls for percentage of correct hits (patients 95.9% SD[6.3%]; controls 98.8% SD[2.9%], $t(68)=.8168$, $p < .3918$), percentage of novel stimuli correctly rejected (patients 96.5% SD[4.6%]; controls 97.4% SD [4.3%], $t(68)=.3591$, $p < .7206$), percentage of standard stimuli correctly rejected (patients

99.7% SD [1.3%]; controls 99.9% SD[0.5%], t(68)=.9019, p < .3703). Significant differences were found in response time to target stimuli where healthy controls were greater than patients (patients = 391.38 seconds SD[67.96s]; controls = 486.28 seconds SD[127.02s] t(68)=3.8974, p < .0002).

Within Group Analysis - Healthy Controls

In the within group analysis for healthy controls, the highest areas of significance were found in the medial (t=13.3/13.6 in the left and right hemispheres respectively) and superior frontal gyrus (t=12.6/12.3), followed by the superior temporal gyrus (t=12.3/10.2). Significant levels of correlation were found in the anterior cingulate (t=8.1/7.8), precuneus (t=8.8/10.7), inferior parietal lobule (t=11.1/10.5), pre-central (t=8.9/10.9) and post-central gyrus (t=9.8/12.3). Subcortical structures such as the thalamus (t=8.9/9.2), insula (t=11.3/10.6), and hippocampus (t=7.9/8.7) were also found to be significant. See Table 1 for a full listing of their talairach coordinates, their area of significance, and maximum t-values (Figure 2).

Within Group Analysis - Patients with Schizophrenia

In the within-group analysis for patients with schizophrenia, the highest areas of significance were found in bilateral temporal lobes (t=17.5/18.5). Significant areas of correlation were also found in the frontal lobe, specifically the anterior cingulate gyrus and medial prefrontal gyrus (t=6.7/9.1). The pre-central (t=5.8/8.2) and post-central (t=7.5/8.5) gyrus were found to be significant in both hemispheres. Subcortical areas such as the thalamus (t=5.9/6.7) and a small portion of the cingulate gyrus were also significant (t=7.4/8.2). See Table 2 for a full listing of their talairach coordinates, their area of significance, and maximum t-values (Figure 3).

Between Group Analyses

A second-level between-group analysis was performed on the results from the IPC algorithm to determine significant activations between healthy controls and patients. The results showed that there were similar patterns of correlation between healthy controls and paranoid schizophrenics, but consistent with our hypothesis there were significant differences in range and significance across major areas of the brain, including bilateral temporal lobes, medial frontal gyrus, parietal lobules, anterior cingulate, dorsolateral prefrontal cortex, thalamus and cerebellum. The greatest differences between the two groups were found in the medial frontal gyrus (t=6.4/6.3) and the insula (t=6.1/5.2). The superior temporal gyrus (t=5.8/5.1), thalamus (t=4.0/3.9), parahippocampus (t=5.0/4.2), anterior cingulate (t=4.6/4.7), and inferior parietal lobule (t=5.0/4.3) were all found to be significant as well. No significant activations were found for patients > healthy controls under our specified FDR threshold. See Table 3 for a full listing of their Talairach coordinates, area of significance, and maximum t-values (Figure 4).

Individual Subject Analysis

Within each subject's correlation maps there were consistent patterns of activation within healthy controls and patients. Overall, correlation maps for healthy controls showed more robust activation at the same threshold (z=3) in comparison to schizophrenics performing the same task (See Figure 5). Common areas of significance were bilateral temporal lobes followed by medial frontal gyrus and pre-central gyrus.

Clustering

The assigned colors from each cluster correspond to the same line colors found in the event related averages for both groups. Results from the cluster map for healthy controls showed the red and cyan cluster were composed of bilateral temporal lobes, thalamus, medial frontal gyrus, and anterior cingulate. The blue and purple clusters grouped around regions near the precentral

and post-central gyrus, while the green cluster comprised of small regions within the occipital lobe.

Results from the cluster map for patients showed the blue cluster was composed mostly of bilateral temporal lobes and small areas of the thalamus. The purple cluster involved the right temporal lobe, medial frontal gyrus, thalamus, and anterior cingulate The green cluster was composed of small regions within the occipital lobe and cerebellum while the red and cyan clusters grouped together around the pre-central and post-central gyrus.

Event related averages for patients and healthy controls were calculated for target responses during an auditory oddball task. Purple clusters corresponded to the greatest signal change, followed by cyan, red, green, and blue clusters. Patients showed significant differences in signal strength in terms of their maximum values than healthy controls. Healthy controls depicted a 0.4% maximum signal increase versus a 0.27% signal increase for patients. Patients and healthy controls showed a similar hemodynamic response in terms of their shape, though patients showed a distinct grouping for the last three clusters of interest (Figure 6 & 7).

DISCUSSION

The main benefits of the IPC algorithm is that it is a data-driven model that attempts to determine the level of fMRI BOLD synchrony within a group of subjects. The IPC is a useful complementary tool since the questions it asks differ from popular approaches such as the GLM, which attempts to find significant brain activity that is relevant to its experimental model. The IPC is concerned with regions of the brain that are commonly utilized for a given task. If a certain region is consistently activating along with a task, then it is likely that it will be found to be significant using the IPC approach even if the activation does not track smoothly with the task. The previous IPC approach focused on its comparison to the GLM method used in SPM2. Here, we have presented a modified IPC algorithm that provides a number of new enhancements to the original IPC algorithm and have utilized it to compare a group of patients with paranoid schizophrenia against healthy controls.

The first modification is that we utilized the IPC method at the level of group comparisons. The previous IPC approach was used for a single within-group comparison and used an empirical threshold rather than a statistical one. The application of U-statistics allows us to use a non-parametric approach to determine statistical significance in the within-group and between-group analyses. The resulting t-values can be easily converted to probability values at each voxel which can then undergo an FDR correction for multiple comparisons. The FDR threshold that we applied from the resulting t-values were thresholded at a higher value for the within-group analyses (FDR, $p<.00005$) based on the strength of our findings while the between-group analysis was subjected to a much lower threshold (FDR, $p<.005$). This is consistent with previous schizophrenia research that has shown much stronger effects in the within-group analysis than the between-group analysis during an auditory oddball task (Kiehl and Liddle 2001; Kiehl, et al. 2005a). The second modification deals with performing the initial correlation by regressing the datasets by their sessions rather than concatenating them and treating it as a single session. By regressing each session with one another, we try to account for variances that might exist in between session. For example, the range of the amplitude signal might differ between the first and second sessions and if the two were concatenated and regressed as a single session, these differences might not be taken into account.

Two neighboring voxels might contain very different signals, but can be both highly significant from the IPC analysis and contain similar t-values. In a more extreme case, these neighboring voxels might be completely associated with very different tasks. Since the IPC approach does not attempt to answer questions regarding the synchrony between voxels *within* a participant,

we used a clustering method to group brain regions that contained similar time-courses. The clustering approach is useful in grouping these time-courses together and delineating an area of interest that can be further scrutinized. The results of our clustering approach shows that patients tend to have clusters that are more homogenous throughout task-related regions within the brain in comparison to healthy controls. One interesting finding can be seen in how patients cluster bi-lateral temporal lobes along with the anterior cingulate and other nearby areas within that particular slice, while the healthy controls tend to delineate the anterior cingulate specifically away from the rest of those regions. The event related averages for patients also showed a significant decrease in amplitude when compared to healthy controls for target responses, especially in the anterior cingulate and bi-lateral temporal lobes. This suggests that patients were not activating as strongly as healthy controls for task-related activities even though they followed a similar hemodynamic response.

Our initial hypothesis stated that healthy controls would show a stronger level of inter-participant synchrony in areas related to auditory target detections. These hypotheses were confirmed, as strong differences were found in bilateral temporal lobes, dorsolateral prefrontal cortex, anterior cingulate, inferior parietal lobules as well as subcortical systems such as the thalamus and parahippocampus. These findings complement current models of schizophrenia such as the frontotemporal disconnection model and the heteromodal association cortex (HASC) model (Friston 1999; Pearlson, et al. 1996). The frontotemporal disconnection hypothesis model focuses on the interconnections between the prefrontal cortex and bilateral temporal lobes. This is consistent with our findings from the between-group analysis which showed the medial frontal gyrus (t=6.4/6.3) and superior temporal lobes bilaterally (t=5.8/5.1) as being highly significant, which implies that patients are not utilizing these areas of the brain as consistently as healthy controls. The HASC model attempts to link schizophrenia as a dysfunction of the heteromodal association cortex, which comprises primarily of the pre-frontal cortex, superior temporal, and inferior parietal cortices. Those same areas were found to be implicated in our between-group analysis. Though these models deal with the interconnectivity between brain regions, our analysis has shown that similar areas are implicated in BOLD synchrony at the voxel-level. Furthermore, our clustering analysis shows that some of these regions may be valuably grouped together on the basis of their time-course similarities.

A confound in the interpretation of our results could be that the experimental paradigm does not consistently activate a specific neural network and allocates random resources of the brain. For example, a resting state task that requires the patient to stare at a blank screen for a few minutes might recruit any number of neural resources at a given moment, making the IPC method difficult to apply. If the activations are not consistent across time, then IPC will not be able to find a strong correlation in those voxels. In such cases, an alternative method would be to implement something like independent component analysis or a similar data-driven approach that could overcome such obstacles (Calhoun and Adali 2006; Jafri, et al. 2007).

The question of how similar the time-courses are within a region is very pertinent and we attempted to answer this by using a clustering algorithm to group these areas together. However, the algorithm is hindered by the fact that the number of clusters specified for the algorithm might not take into account the more subtle inter-relationships that exist between these regions. A pairwise correlation between every voxel of interest could be performed to more directly assess interregional connectivity. Future possibilities in answering these questions might utilize tools within probability theory such as structural equation modeling or dynamic Bayesian networks, which recently have been successfully applied to neuroimaging data to determine relationships between specific brain regions of interest (Burge and Lane 2005; Friston, et al. 2003; McIntosh and Gonzalez-Lima 1994).

Conclusion

By utilizing a novel data-driven correlation approach to fMRI data, we were able to uncover many distinct brain regions that point to a lack of inter-participant synchrony within paranoid schizophrenics that correlate with previous fMRI studies of schizophrenia. Improvements were made to the original algorithm to improve the robustness of our results and to perform statistically valid group comparisons that shed new light on the differences between patients with schizophrenia and healthy control populations. The IPC method in general is an excellent tool in complementing popular approaches to fMRI such as GLM and ICA as it attempts to look at a different aspect of BOLD activity, namely inter-participant neural synchrony. Our approach is general and can be applied to any study which involved comparisons of groups.

ACKNOWLEDGEMENTS

This work was supported by the National Institutes of Health (1 R01 EB 000840-01 and 1 R01 EB 005846-01 to V.C., 5 R01 MH43775-08, 5 R01 MH43775-08 to G.P, and 5 R01 MH072681-08 to K.K). We would like to thank Dr. Oguz Demirci for his assistance in the clustering section of this article, Emily K Bell for her help in organizing the patient's behavioral scores and medications list, and Dr. Matthew Shane for help in editing.

References

Ashburner J, Friston KJ. Nonlinear spatial normalization using basis functions. Hum Brain Mapp 1999;7 (4):254–266. [PubMed: 10408769]

Breakspear M, Terry JR, Friston KJ, Harris AW, Williams LM, Brown K, Brennan J, Gordon E. A disturbance of nonlinear interdependence in scalp EEG of subjects with first episode schizophrenia. NeuroImage 2003;20(1):466–478. [PubMed: 14527607]

Burge, J.; Lane, T. Learning Class-Discriminative Dynamic Bayesian Networks. Germany: Bonn; 2005. p. 97-104.

Calhoun VD, Adali T. 'Unmixing' Functional Magnetic Resonance Imaging with Independent Component Analysis. IEEE Eng. in Medicine and Biology 2006;25(2):79–90.

Calhoun VD, Adali T, Giuliani NR, Pekar JJ, Kiehl KA, Pearlson GD. Method for multimodal analysis of independent source differences in schizophrenia: combining gray matter structural and auditory oddball functional data. Hum Brain Mapp 2006;27(1):47–62. [PubMed: 16108017]

Calhoun VD, Kiehl KA, Liddle PF, Pearlson GD. Aberrant localization of synchronous hemodynamic activity in auditory cortex reliably characterizes schizophrenia. Biol Psychiatry 2004;55(8):842–849. [PubMed: 15050866]

Duda, RO. Pattern Classification. John Wiley & Sons, Inc; 2001.

First, MD.; Spitzer, RL.; Gibbon, M.; Williams, JBW. Biometrics Research Department. New York: New York State Psychiatric Institute; Structured Clinical interview for DSM-IV axis I disorders-patient edition (SCID-I/P, Version 2.0).

Freire L, Mangin JF. Motion correction algorithms may create spurious brain activations in the absence of subject motion. NeuroImage 2001;14(3):709–722. [PubMed: 11506543]

Freire L, Roche A, Mangin JF. What is the best similarity measure for motion correction in fMRI time series? IEEE Trans Med Imaging 2002;21(5):470–484. [PubMed: 12071618]

Friston K, Holmes A, Worsley K, Poline J, Frith C, Frackowiak R. Statistical parametric maps in functional imaging: a general linear approach. Hum Brain Mapp 1995a;(2):189–210.

Friston KJ. The disconnection hypothesis. Schizophr. Res 1998;30(2):115–125. [PubMed: 9549774]

Friston KJ. Schizophrenia and the disconnection hypothesis. Acta Psychiatr. Scand. Suppl 1999;395:68–79. [PubMed: 10225335]

Friston KJ, Frith CD, Turner R, Frackowiak RS. Characterizing evoked hemodynamics with fMRI. Neuroimage 1995b;2(2):157–165. [PubMed: 9343598]

Friston KJ, Harrison L, Penny W. Dynamic causal modelling. NeuroImage 2003;19(4):1273–1302. [PubMed: 12948688]

Friston KJ, Holmes AP, Poline JB, Grasby PJ, Williams SC, Frackowiak RS, Turner R. Analysis of fMRI time-series revisited. Neuroimage 1995c;2(1):45–53. [PubMed: 9343589]

Genovese CR, Lazar NA, Nichols T. Thresholding of statistical maps in functional neuroimaging using the false discovery rate. Neuroimage 2002;15(4):870–878. [PubMed: 11906227]

Harabasz, Ca. A Dendrite Method for Cluster Analysis Communications in Statistics 1974;3(1):1–27.

Hejnar MP, Kiehl KA, Calhoun VD. Interparticipant correlations: A model free FMRI analysis technique. Hum Brain Mapp. 2006

Jafri M, Pearlson GD, Calhoun VD. Aberrant Connectivity Among Spatially Independent Resting-State Networks in Schizophrenia. NeuroImage. 2007

Job DE, Whalley HC, McConnell S, Glabus M, Johnstone EC, Lawrie SM. Structural gray matter differences between first-episode schizophrenics and normal controls using voxel-based morphometry. Neuroimage 2002;17(2):880–889. [PubMed: 12377162]

Kiehl KA, Liddle PF. An event-related functional magnetic resonance imaging study of an auditory oddball task in schizophrenia. Schizophr. Res 2001;48(2–3):159–171. [PubMed: 11295369]

Kiehl KA, Stevens MC, Celone K, Kurtz M, Krystal JH. Abnormal hemodynamics in schizophrenia during an auditory oddball task. Biol Psychiatry 2005a;57(9):1029–1040. [PubMed: 15860344]

Kiehl KA, Stevens MC, Celone K, Kurtz M, Krystal JH. Abnormal hemodynamics in schizophrenia during an auditory oddball task. Biological Psychiatry 2005b;57(9):1029–1040. [PubMed: 15860344]

Kubicki M, McCarley R, Westin CF, Park HJ, Maier S, Kikinis R, Jolesz FA, Shenton ME. A review of diffusion tensor imaging studies in schizophrenia. J Psychiatr Res 2007;41(1–2):15–30. [PubMed: 16023676]

Laurens KR, Kiehl KA, Ngan ET, Liddle PF. Attention orienting dysfunction during salient novel stimulus processing in schizophrenia. Schizophr Res 2005;75(2–3):159–171. [PubMed: 15885507]

Lawrie SM, Buechel C, Whalley HC, Frith CD, Friston KJ, Johnstone EC. Reduced frontotemporal functional connectivity in schizophrenia associated with auditory hallucinations. Biological Psychiatry 2002;51(12):1008–1011. [PubMed: 12062886]

McIntosh AR, Gonzalez-Lima F. Structural Equation Modeling and Its Application to Network Analysis in Functional Brain Imaging. Hum. Brain Map 1994;2:2–22.

Ngan ET, Vouloumanos A, Cairo TA, Laurens KR, Bates AT, Anderson CM, Werker JF, Liddle PF. Abnormal processing of speech during oddball target detection in schizophrenia. Neuroimage 2003;20(2):889–897. [PubMed: 14568459]

Pearlson GD, Petty RG, Ross CA, Tien AY. Schizophrenia: a disease of heteromodal association cortex? Neuropsychopharmacology 1996;14(1):1–17. [PubMed: 8719025]

Rajapakse JC, Kruggel F, Maisog JM, von Cramon DY. Modeling hemodynamic response for analysis of functional MRI time-series. Hum Brain Mapp 1998;6(4):283–300. [PubMed: 9704266]

Randles, RH.; Wolfe, DA. Introduction to the Theory of Nonparametric Statistics. John Wiley and Sons, Inc; 1979.

Stevens M, Calhoun VD, Kiehl KA. Hemispheric Differences in Hemodynamics Elicited by Auditory Oddball Stimuli. NeuroImage 2005;26(3):782–792. [PubMed: 15955488]

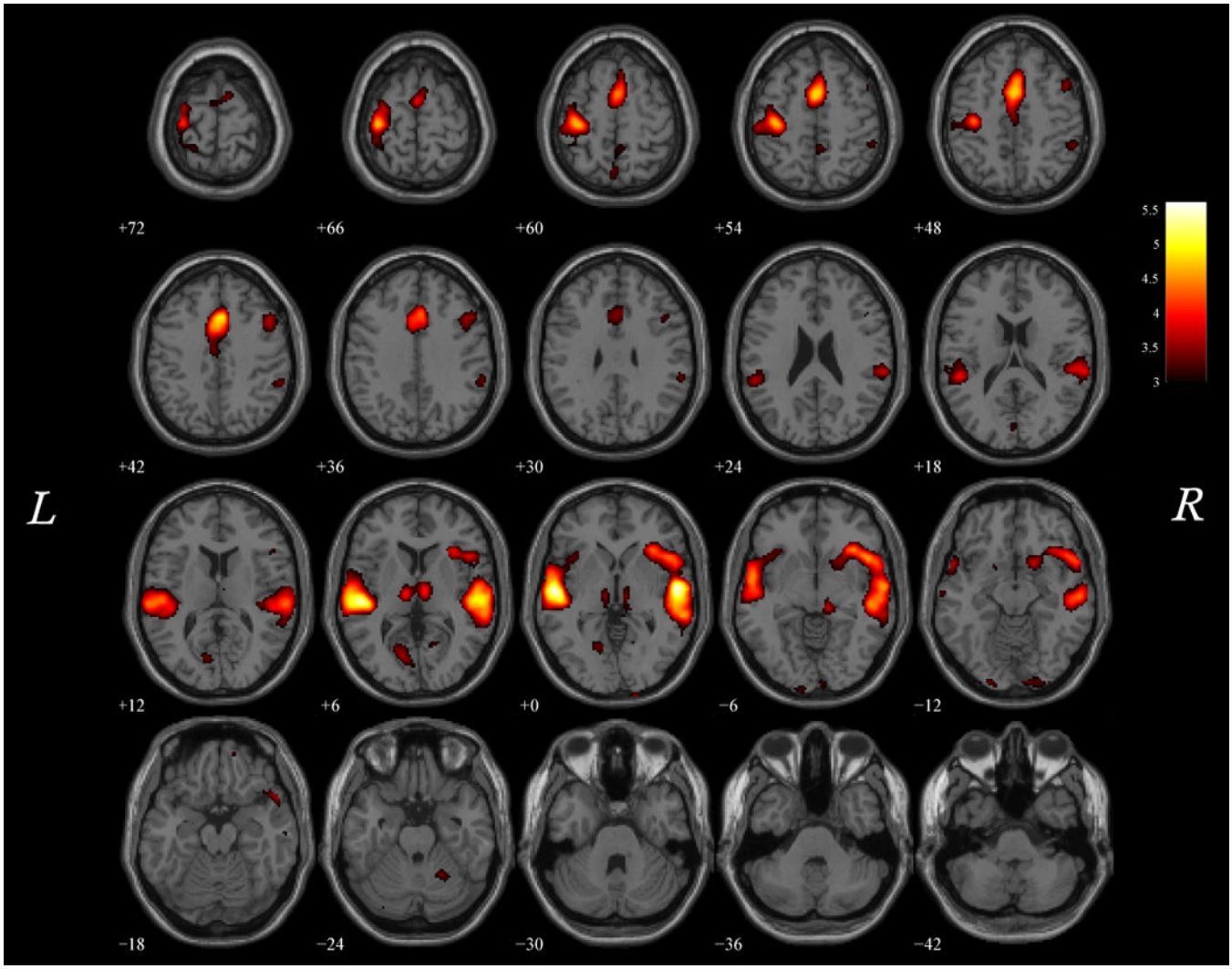

Figure 1.
Sample correlation map from healthy control participant #1

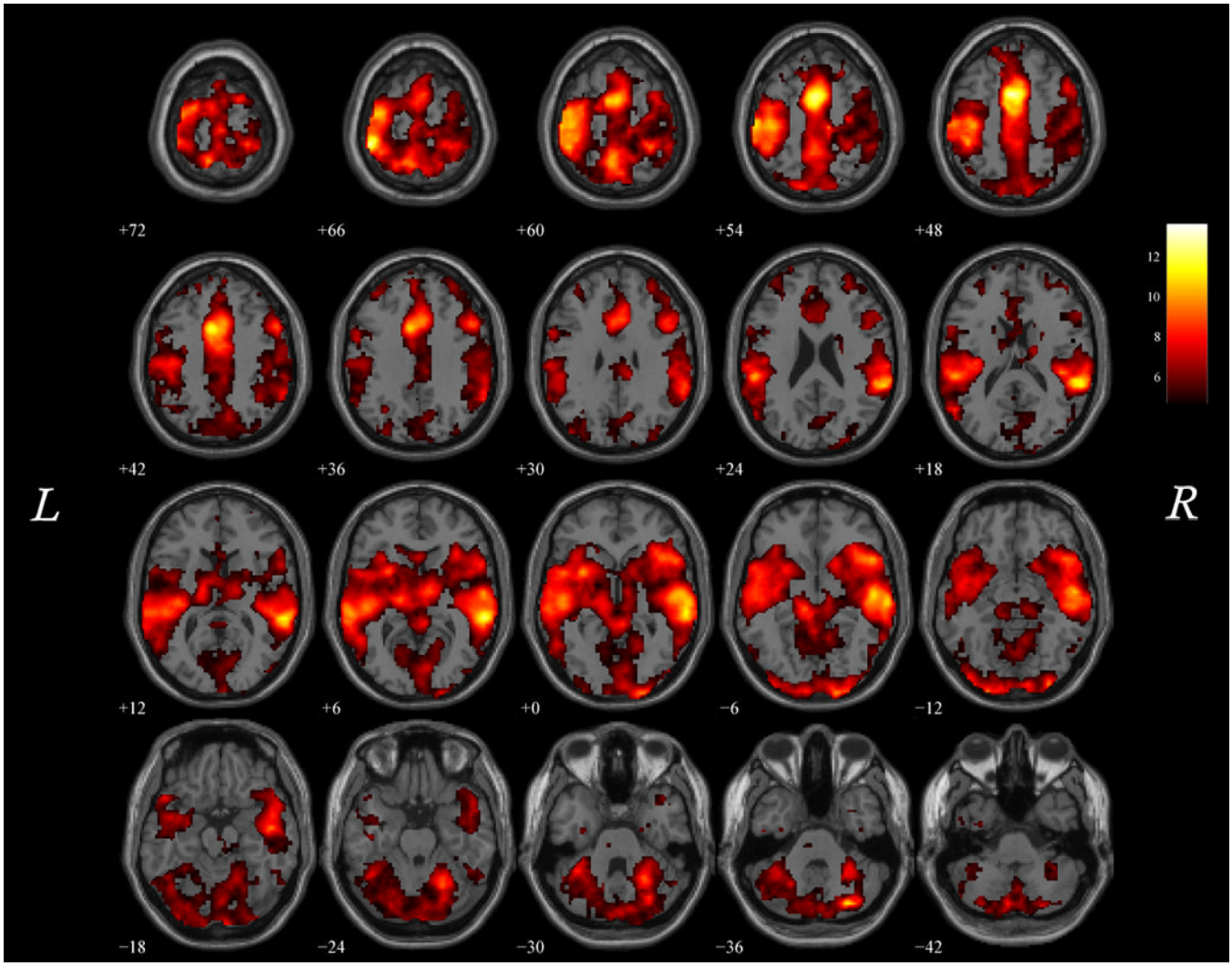

Figure 2.
IPC - Healthy (FDR p < .00005)

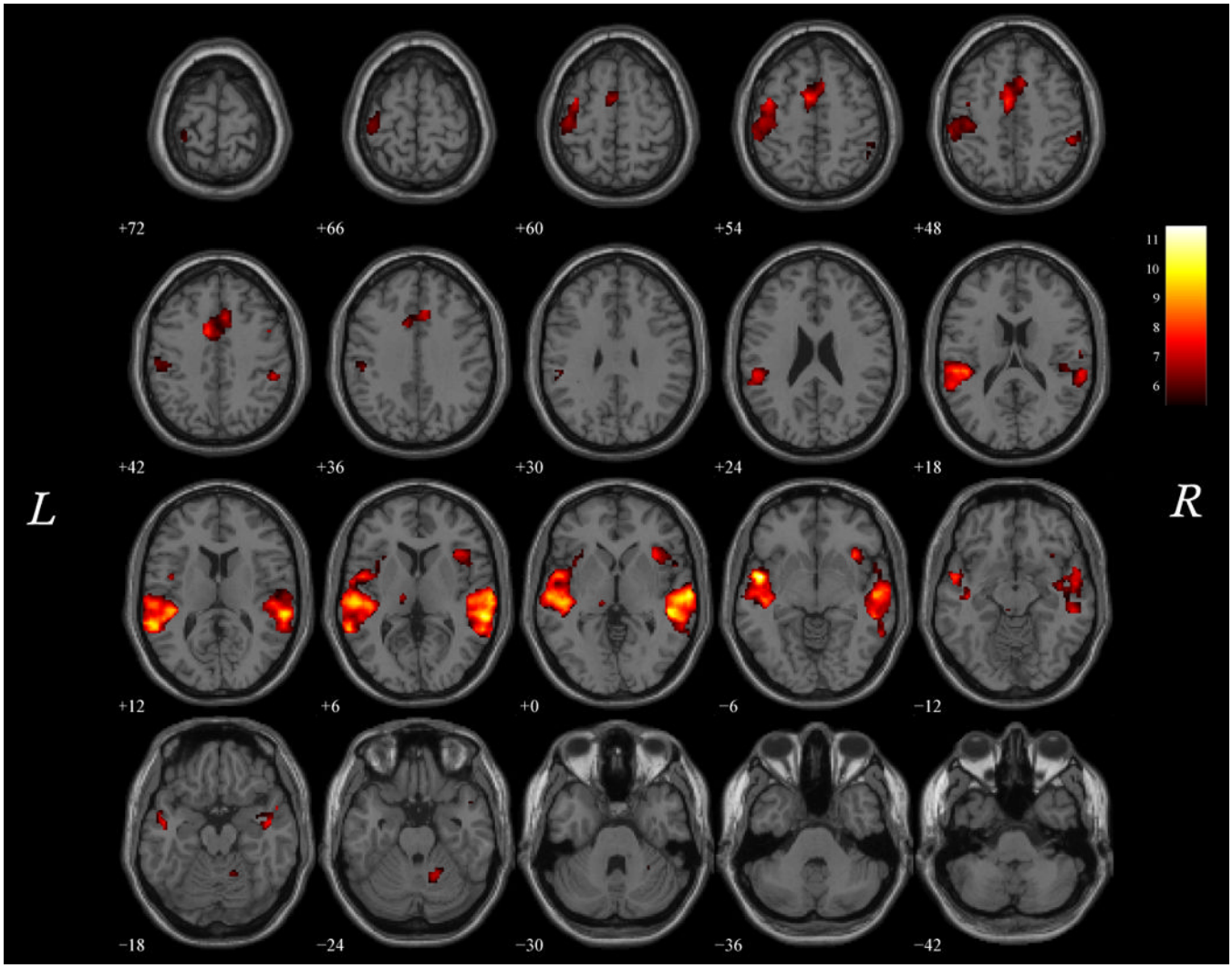

Figure 3.
IPC - Patients (FDR p < .00005)

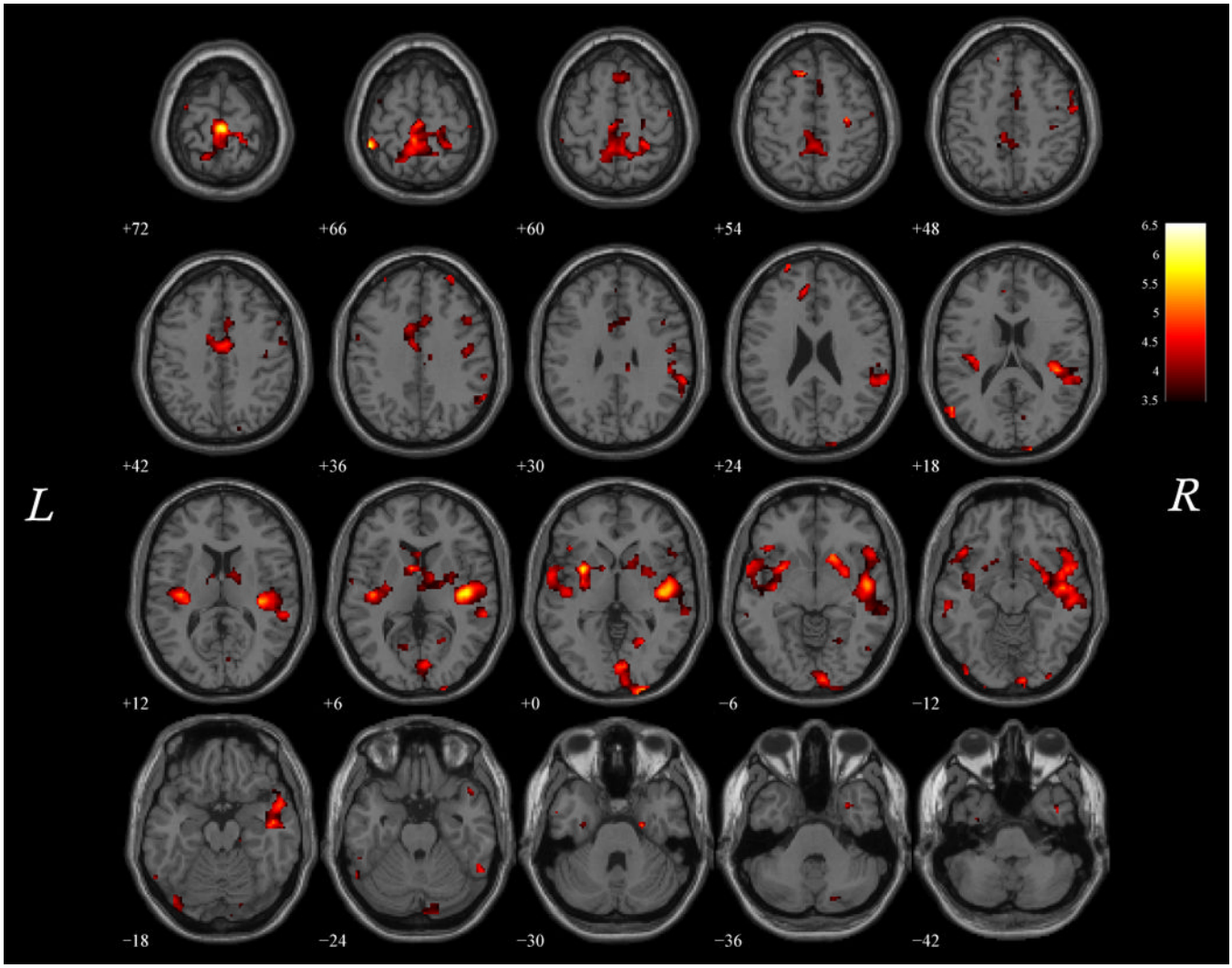

Figure 4.
IPC – Group Healthy > Patients (FDR p <.005)

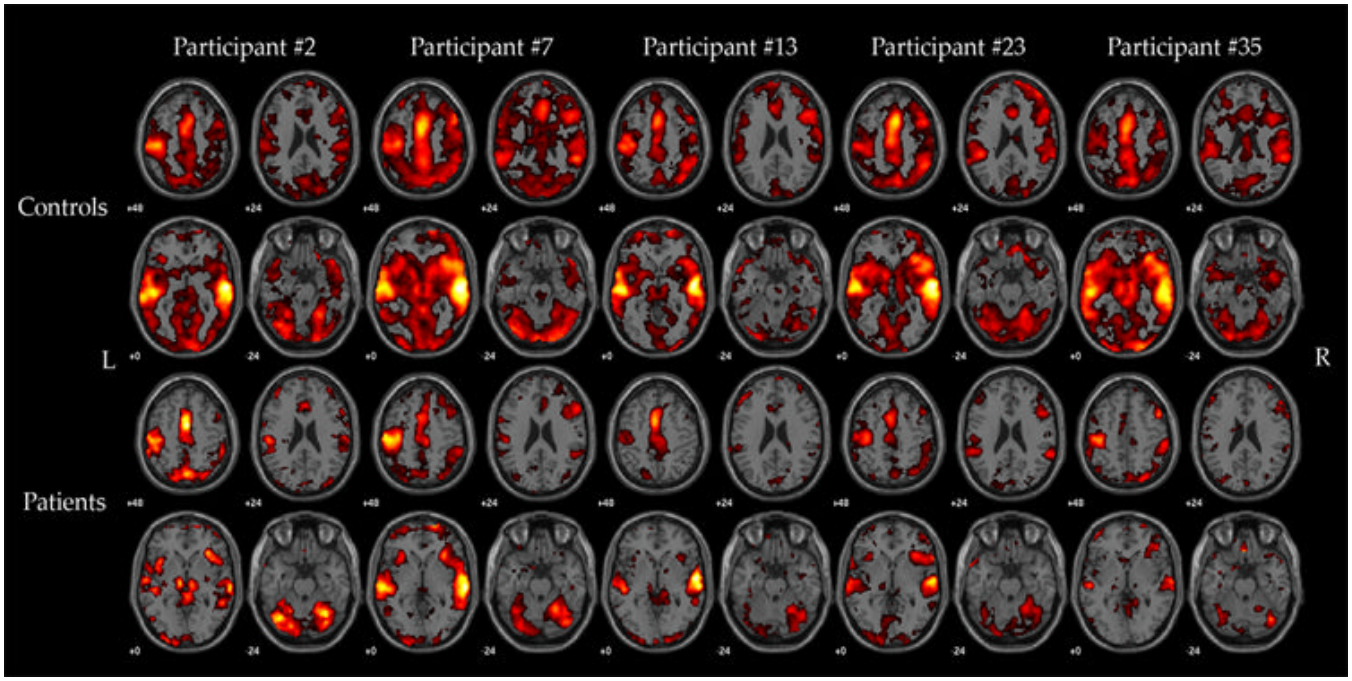

Figure 5.
Correlation Samples from Schizophrenics and Healthy Controls

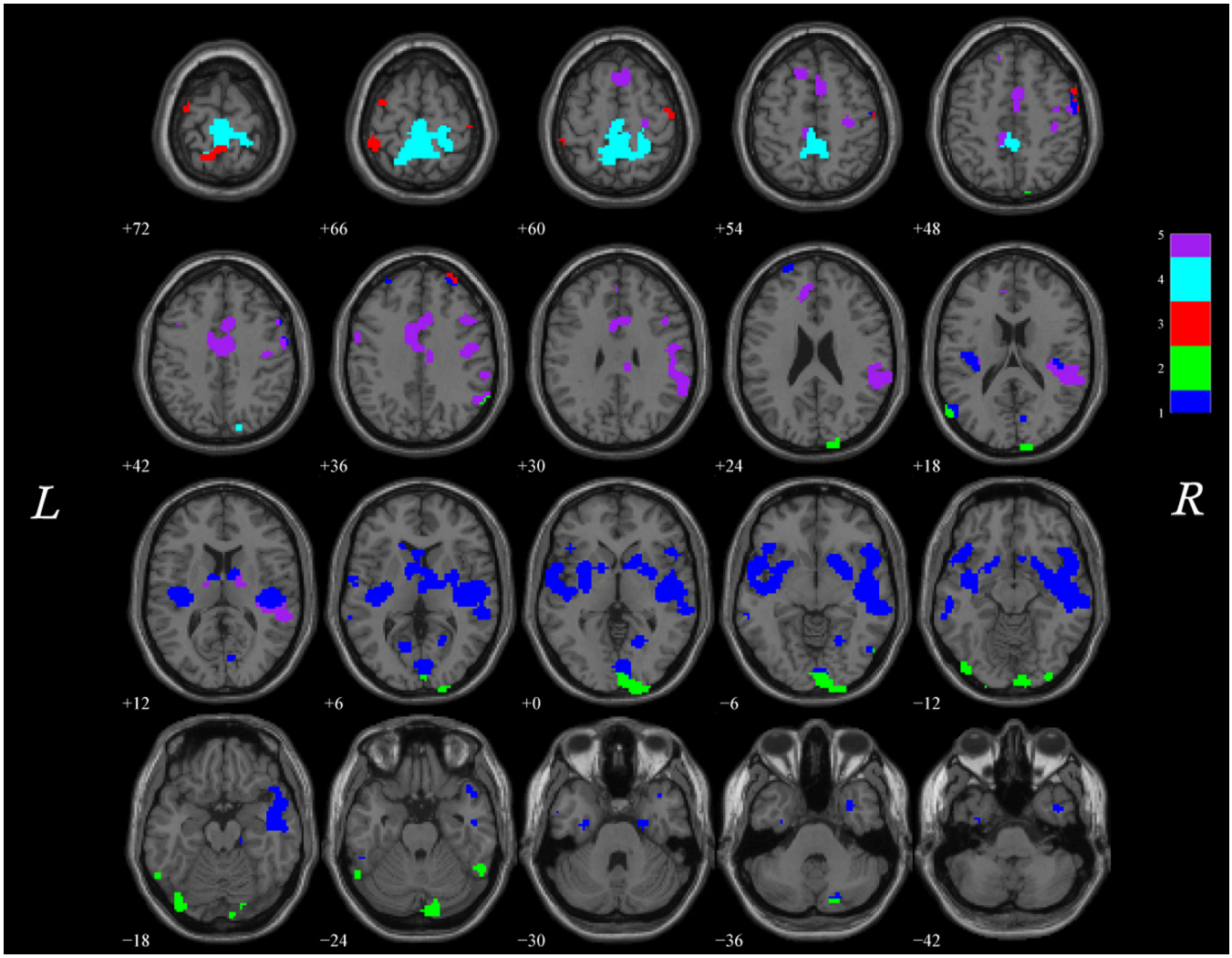

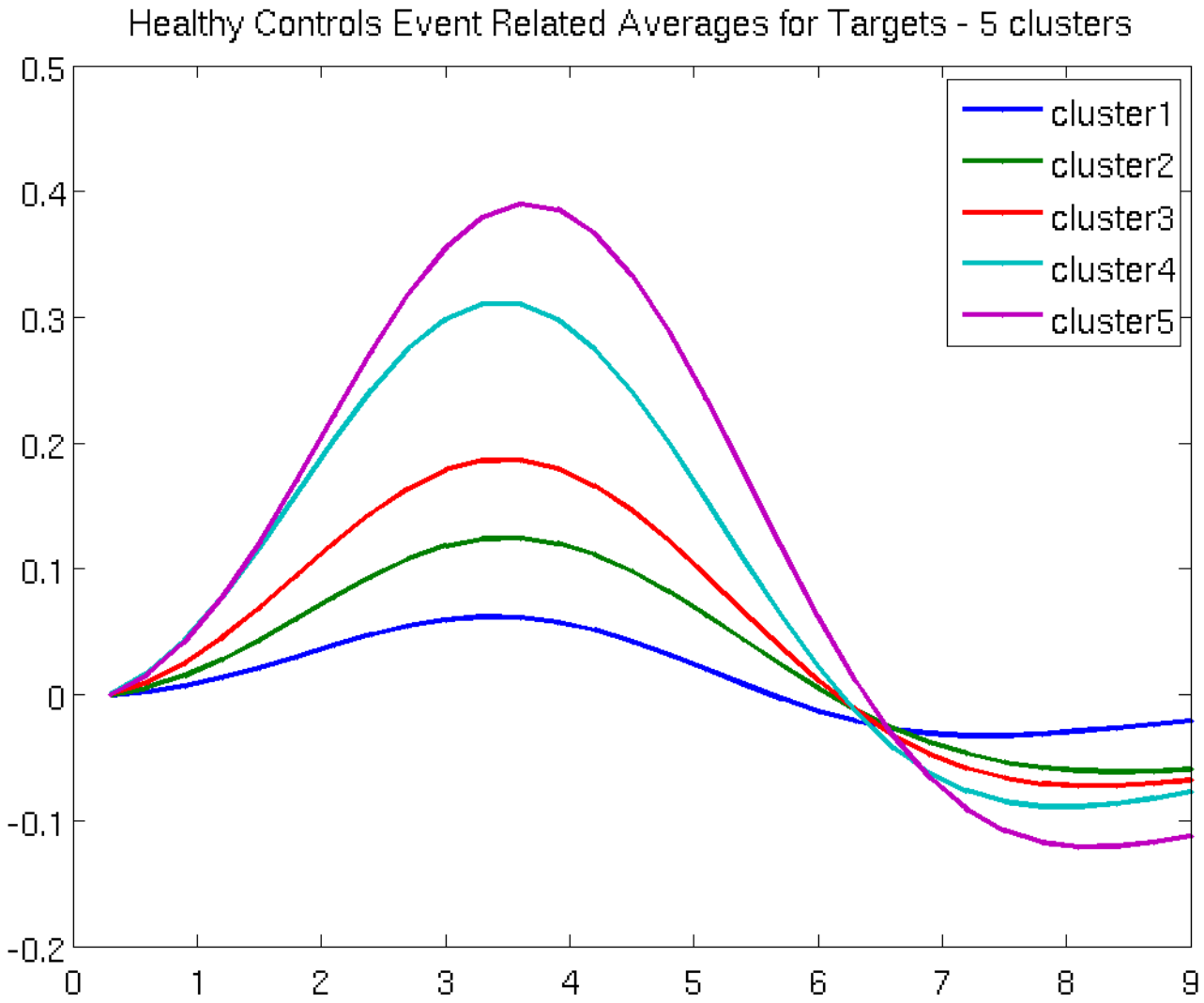

Figure 6.
Event Related Averages for Targets - Five Cluster Results for Healthy Controls

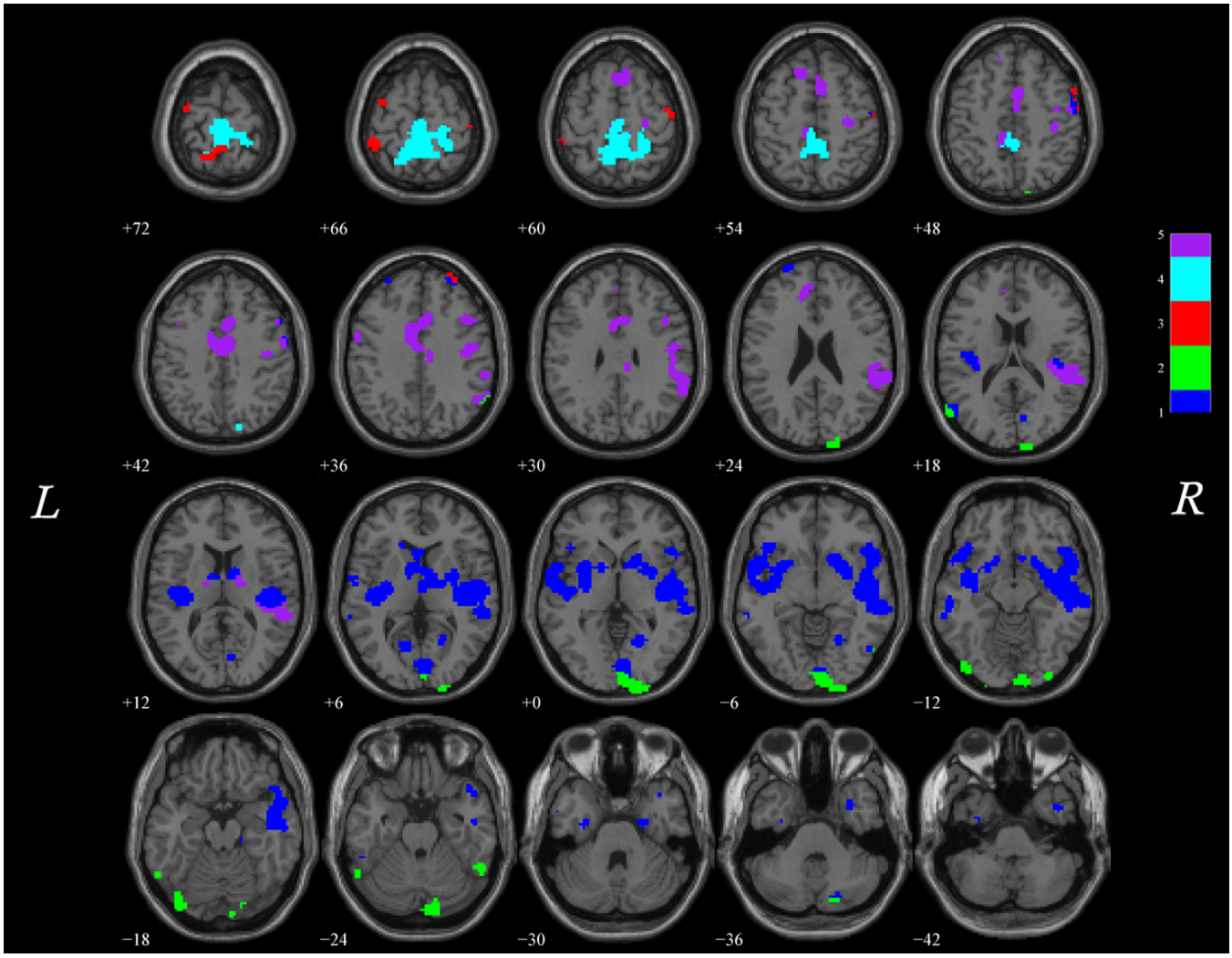

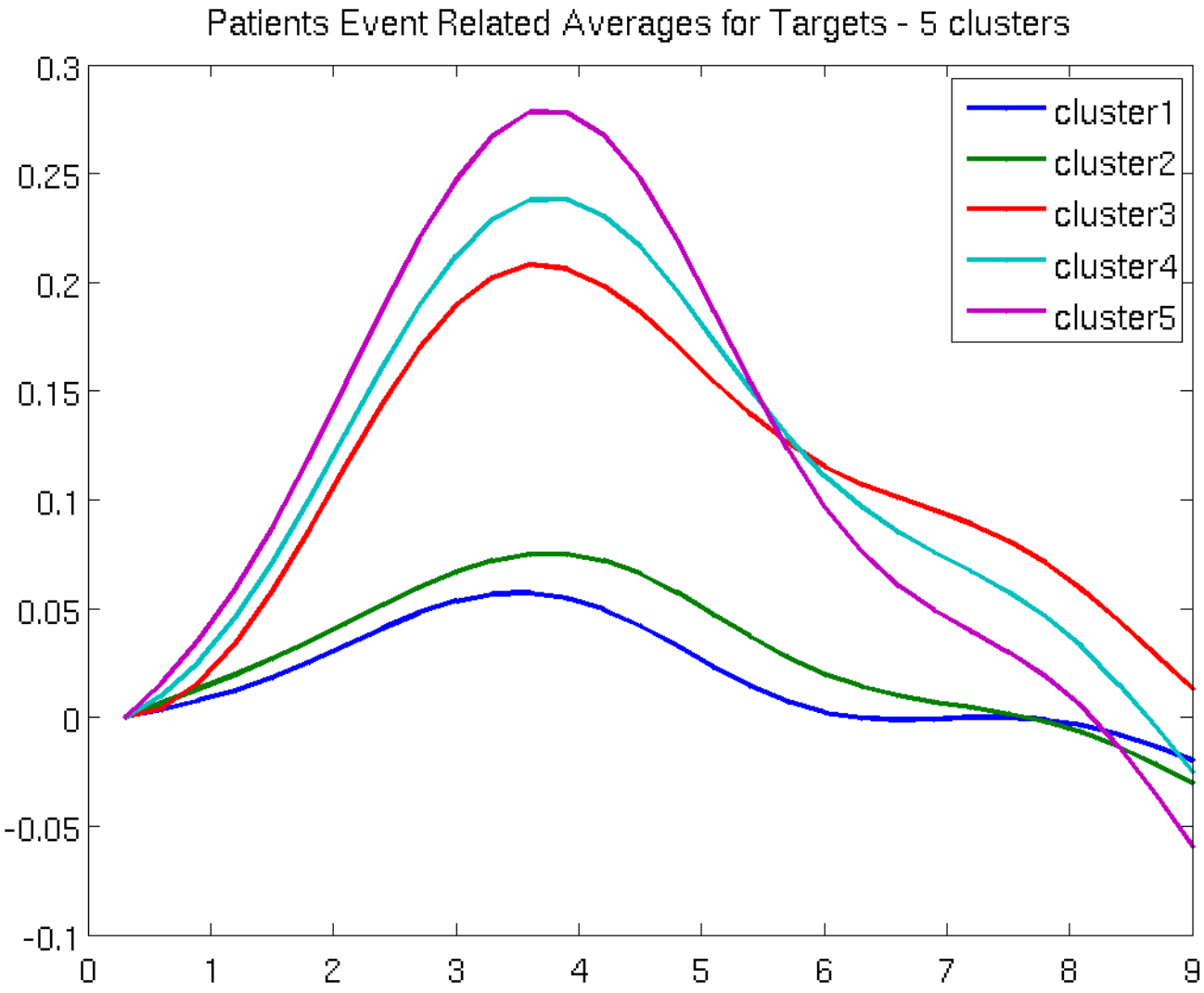

Figure 7.
Event Related Averages for Targets - Five Cluster Results for Patients

Table 1

Talairach Coordinates for 1-sample U-statistics for Healthy Controls

Area (Positive Activation)	Brodmann Areas	R/L volume (mm^3)	R/L random effects Max T
Medial Frontal Gyrus	32, 6, 8, 9, 10, 11	13.5/12.6	13.6(0,8,47)/13.3(3,8,47)
Superior Frontal Gyrus	6, 8, 9, 10	14.7/15.3	12.6(0,5,49)/12.3(3,5,49)
Superior Temporal Gyrus	22, 21, 13, 42, 41, 38, 39	31.7/30.2	12.3(−59,−34,10)/10.2(59,−32,7)
Postcentral Gyrus	2, 1, 3, 4, 5, 40, 7, 43	21.5/21.1	9.8(−30,−38,60)/12.3(39,−32,62)
Cingulate Gyrus	24, 32, 9, 31, 23	17.9/13.3	12.2(−3,2,47)/12.2(6,11,41)
Middle Temporal Gyrus	21, 22, 39, 38, 37, 19, 20	24.5/20.3	11.8(−62,−32,4)/9.4(62,−32,4)
Sub-Gyral	21, 6, 40, 13, 20,Corpus Callosum, 47,Hippocampus, 8, 7	21.6/22.2	11.4(−50,−12,−7)/9.2(36,−18,42)
Insula	13, 41, 22, 40, 47, 45	13.0/14.5	11.3(−56,−37,18)/10.6(53,−31,21)
Cuneus	18, 17, 23, 7, 19, 30	15.0/11.3	11.3(−18,−102,3)/8.3(9,−99,0)
Inferior Parietal Lobule	40, 39, 7	18.1/17.3	11.1(−62,−40,24)/10.5(42,−36,46)
Precentral Gyrus	4, 6, 44, 13, 43, 9, 3	25.5/22.2	8.9(−30,−12,48)/10.9(36,−21,48)
Precuneus	7, 19, 31, 39	18.5/13.6	8.8(−6,−61,58)/10.7(3,−52,61)
Middle Frontal Gyrus	6, 8, 9, 46, 10, 47	22.5/13.3	9.5(−50,13,35)/10.4(33,−6,61)
Paracentral Lobule	5, 31, 6, 4, 7	5.8/4.8	10.2(0,−9,45)/10.0(3,−9,45)
Inferior Occipital Gyrus	18, 17, 19	3.0/4.1	10.2(−33,−96,−3)/8.8(39,−91,−6)
Inferior Frontal Gyrus	47, 9, 45, 44, 13, 46	17.8/9.9	10.2(−50,17,−6)/7.5(42,14,−11)
Extra-Nuclear	47,Corpus Callosum, 13,Pulvinar,Lateral Globus Pallidus, Putamen	17.9/18.1	8.7(−36,23,−1)/9.9(30,6,0)
Lingual Gyrus	18, 17, 19	10.8/8.4	8.8(−27,−99,−3)/9.5(24,−99,−5)
Lentiform Nucleus	Putamen,Lateral Globus Pallidus, Medial Globus Pallidus	7.5/8.3	8.1(−18,11,−8)/9.3(27,6,2)
Transverse Temporal Gyrus	41, 42	1.5/1.8	8.7(−48,−26,10)/9.3(45,−29,10)
Thalamus		5.6/6.4	8.9(−12,−11,6)/9.2(15,−17,6)
Middle Occipital Gyrus	18, 37, 19	5.9/4.8	9.0(−21,−99,5)/8.0(39,−93,0)
Supramarginal Gyrus	40	4.9/4.6	8.9(−59,−42,27)/7.2(50,−42,30)
Parahippocampal Gyrus	30,Amygdala, 27, 34, 35, 19, 36, 18,Hippocampus, 37, 28	4.5/3.5	7.9(−9,−41,5)/8.7(12,−32,−1)
Claustrum		1.4/1.4	7.1(−33,9,0)/8.3(30,11,−3)
Anterior Cingulate	24	2.9/3.1	8.1(−3,16,24)/7.8(3,19,24)
Superior Parietal Lobule	7	3.9/3.5	7.5(−18,−49,61)/8.0(36,−47,60)
Fusiform Gyrus	37	4.6/6.8	6.4(−21,−79,−14)/7.8(42,−50,−18)
Caudate	Caudate Tail	1.3/1.6	6.5(−6,3,0)/7.8(36,−15,−7)
Lateral Ventricle		2.5/2.5	7.5(−3,18,7)/7.2(6,−2,11)
Subcallosal Gyrus	13, 34, 47	0.6/0.5	7.4(−18,11,−11)/6.7(24,8,−11)
Inferior Temporal Gyrus	21, 20, 37, 19, 18	2.8/2.4	7.1(−56,−12,−15)/6.9(53,−2,−30)
Superior Occipital Gyrus	19	1.1/0.6	6.5(−33,−83,29)/7.0(42,−80,32)
Uncus	20, 28	0.5/0.6	5.8(−24,−10,−27)/6.8(33,−13,−27)
Posterior Cingulate	30, 29, 31, 23	2.9/2.3	6.7(−6,−43,8)/6.0(3,−43,8)
Angular Gyrus	39	0.7/0.6	6.1(−48,−56,36)/6.0(53,−56,36)

Table 2

Talairach Coordinates for 1-sample U-statistics for Patients

Area (Positive Activation)	Brodmann Areas	R/L volume (mm^3)	R/L random effects Max T
Superior Temporal Gyrus	22, 42, 41, 21, 13, 38	17.1/18.5	10.9(−62,−34,10)/11.4(48,0,−5)
Middle Temporal Gyrus	22, 21, 37, 39	11.6/3.9	10.6(−50,−32,2)/9.3(59,−46,8)
Sub-Gyral	21, 13	3.6/3.2	7.9(−45,−9,−15)/9.5(39,−18,−7)
Transverse Temporal Gyrus	41, 42	1.0/1.5	8.2(−50,−23,12)/9.3(42,−31,13)
Middle Frontal Gyrus	6, 9, 46, 8, 10	1.1/1.9	6.7(−45,8,38)/9.1(39,2,47)
Insula	13, 22, 40, 47, 41	2.6/7.0	7.8(−36,20,2)/8.9(42,−20,1)
Postcentral Gyrus	40, 2, 3, 43, 1, 5	1.9/8.8	7.5(−50,−30,37)/8.5(53,−28,21)
Cingulate Gyrus	32, 24, 31	3.6/3.9	7.4(−9,25,32)/8.2(9,8,38)
Inferior Frontal Gyrus	47, 45, 9, 44	3.5/0.2	8.2(−36,20,−6)/5.8(33,23,−4)
Extra-Nuclear	47, 13	0.2/1.4	7.7(−36,20,−1)/8.2(48,0,3)
Precentral Gyrus	44, 6, 13, 43	0.3/6.2	5.9(−42,18,7)/8.2(48,0,6)
Medial Frontal Gyrus	6, 32, 9, 8	1.9/2.0	7.1(0,2,50)/8.0(6,5,49)
*	Dentate,Subthalamic Nucleus,Substania Nigra	0.6/0.1	7.2(−65,−52,11)/7.7(50,3,3)
Inferior Parietal Lobule	40	2.7/2.9	7.6(−50,−30,40)/7.6(53,−31,24)
Superior Frontal Gyrus	6, 8	1.3/0.5	7.4(0,5,49)/7.4(3,5,49)
Thalamus		0.4/1.1	5.9(−15,−20,4)/6.7(12,−17,6)

Table 3

Talairach Coordinates for 2-sample U-statistics where Healthy Controls > Patients.

Area (Positive Activation)	Brodmann Areas	R/L volume (mm^3)	R/L random effects Max T
Medial Frontal Gyrus	6, 9, 8, 32, 25, 10	4.7/4.7	6.4(−3,−23,67)/6.3(3,−20,65)
Insula	13, 41, 40, 22, 47	8.2/6.3	6.1(−45,−14,3)/5.2(36,−17,12)
*	Corpus Callosum,Dentate,Red Nucleus	1.3/0.7	5.0(−12,14,−8)/4.8(21,65,19)
Superior Temporal Gyrus	22, 13, 38, 39, 41, 21, 42	21.6/12.5	5.8(−45,−17,6)/5.1(53,−60,20)
Extra-Nuclear	Corpus Callosum, 13,Lateral Globus Pallidus,Putamen	10.5/8.9	5.4(−15,17,−8)/5.7(30,6,0)
Lentiform Nucleus	Putamen,Lateral Globus Pallidus,Medial Globus Pallidus	5.7/5.0	5.2(−18,14,−8)/5.4(27,6,0)
Transverse Temporal Gyrus	41, 42	1.4/0.5	5.4(−39,−23,12)/4.2(39,−23,12)
Sub-Gyral	21, 40, 13, 20	11.1/6.2	5.3(−48,−9,−15)/4.6(36,−12,−7)
Paracentral Lobule	6, 5, 4, 31, 7	3.9/4.1	4.8(−3,−29,65)/5.3(3,−32,62)
Superior Frontal Gyrus	10, 9, 6, 8	5.5/6.8	4.5(−27,54,30)/5.3(9,26,48)
Inferior Occipital Gyrus	18, 17, 19	1.5/2.0	5.1(−33,−94,−5)/5.2(39,−88,−8)
Caudate	Caudate Head,Caudate Body,Caudate Tail	1.2/1.1	4.2(−12,17,−6)/5.1(6,6,5)
Precentral Gyrus	4, 6, 13, 9, 43, 44	15.1/4.7	5.1(−30,−15,50)/4.2(56,−1,36)
Cuneus	17, 18, 19, 23, 30, 7	10.0/1.9	5.1(−3,−81,7)/4.1(9,−64,9)
Middle Temporal Gyrus	39, 21, 38, 22, 19, 37, 20	13.0/10.2	5.1(−53,−12,−12)/5.1(53,−63,20)
Lingual Gyrus	17, 18, 19	7.5/2.2	5.0(−9,−97,−8)/4.2(24,−99,−5)
Claustrum		1.0/0.7	5.0(−36,−14,3)/4.8(33,−17,12)
Parahippocampal Gyrus	35,Hippocampus, 18, 19, 34,Amygdala, 30, 36	2.2/0.8	5.0(−24,−13,−25)/4.2(24,−10,−25)
Inferior Parietal Lobule	40	6.2/1.2	5.0(−62,−36,29)/4.3(50,−32,57)
Precuneus	7, 31, 19	4.6/2.9	5.0(−12,−47,55)/4.4(9,−47,60)
Postcentral Gyrus	2, 5, 3, 7, 1, 40, 43	9.2/4.8	4.9(−27,−35,57)/4.9(45,−32,62)
Fusiform Gyrus	37, 19, 18, 20	1.3/2.2	4.9(−56,−50,−15)/4.8(56,−50,−18)
Middle Frontal Gyrus	10, 9, 6, 8, 47, 46	4.8/2.9	4.7(−45,16,30)/4.9(24,62,19)
Cingulate Gyrus	24, 32, 31, 23	10.4/7.0	4.8(−3,−7,39)/4.8(3,−7,36)
Inferior Frontal Gyrus	47, 9, 45	5.5/4.9	4.6(−50,17,−6)/4.8(42,20,−11)
Subcallosal Gyrus	13, 34, 25, 47, 11	0.8/1.0	4.8(−21,8,−11)/4.2(15,11,−13)
Middle Occipital Gyrus	18, 19, 37	2.5/0.8	4.7(−27,−99,5)/4.6(42,−79,−9)
Anterior Cingulate	32, 24, 25, 33	0.8/1.2	4.6(−9,14,−8)/4.7(9,39,20)
Supramarginal Gyrus	40	2.3/0.7	4.6(−56,−51,33)/3.7(53,−54,36)
Uncus	20, 28	0.7/0.9	4.5(−30,4,−30)/4.5(33,−13,−27)
Inferior Temporal Gyrus	21, 20, 37, 19	1.6/1.9	4.3(−56,−12,−15)/4.5(53,−2,−30)
Superior Parietal Lobule	7, 5	0.5/0.3	4.5(−18,−47,60)/4.0(18,−55,61)
Posterior Cingulate	30, 23, 31, 29	1.5/1.4	4.4(−21,−58,6)/4.1(9,−40,24)
Thalamus		2.2/1.5	4.0(−12,−6,6)/3.9(9,−2,8)
Medial Frontal Gyrus	6, 9, 8, 32, 25, 10	4.7/4.7	6.4(−3,−23,67)/6.3(3,−20,65)